

## RESEARCH LETTER

10.1002/2014GL061095

## Key Points:

- Mechanical and thermal damage effects on radon release are studied in granites
- Measurements of radon concentration in pores are coupled with a triaxial cell
- Mechanical damage connects isolated pores leading to transient radon signals

## Supporting Information:

- Readme
- Figure S1
- Figure S2

## Correspondence to:

A. Nicolas,  
nicolas@geologie.ens.fr

## Citation:

Nicolas, A., F. Girault, A. Schubnel, É. Pili, F. Passelègue, J. Fortin, and D. Deldicque (2014), Radon emanation from brittle fracturing in granites under upper crustal conditions, *Geophys. Res. Lett.*, *41*, 5436–5443, doi:10.1002/2014GL061095.

Received 2 JUL 2014

Accepted 18 JUL 2014

Accepted article online 23 JUL 2014

Published online 4 AUG 2014

## Radon emanation from brittle fracturing in granites under upper crustal conditions

Aurélien Nicolas<sup>1</sup>, Frédéric Girault<sup>1</sup>, Alexandre Schubnel<sup>1</sup>, Éric Pili<sup>2</sup>, François Passelègue<sup>1</sup>, Jérôme Fortin<sup>1</sup>, and Damien Deldicque<sup>1</sup>

<sup>1</sup>Laboratoire de Géologie, École Normale Supérieure, CNRS UMR 8538, Paris, France, <sup>2</sup>CEA, DAM, DIF, Arpajon, France

**Abstract** Radon-222, a radioactive gas naturally produced in the Earth's crust, informs us about the migration of fluids and is sometimes considered as a potential earthquake precursor. Here we investigate the effects of mechanical and thermal damage on the radon emanation from various granites representative of the upper crust. Radon concentration measurements performed under triaxial stress and pore fluid pressure show that mechanical damage resulting from cycles of differential stress intensifies radon release up to  $170 \pm 22\%$  when the sample ruptures. This radon peak is transient and results from the connection of isolated micropores to the permeable network rather than new crack surface creation per se. Heating to  $850^\circ\text{C}$  shows that thermal fracturing irreversibly decreases emanation by 59–97% due to the amorphization of biotites hosting radon sources. This study, and the developed protocols, shed light on the relation between radon emanation of crustal rocks, deformation, and pressure-temperature conditions.

### 1. Introduction

The radioactive gas radon-222 (half-life 3.82 days) is naturally produced in rocks by alpha decay of radium-226. Easily measurable in the field, it is a precious asset that has given information about fluid migration in several volcanically [Richon *et al.*, 2003; Cigolini *et al.*, 2007] and tectonically active areas [Trique *et al.*, 1999; Perrier *et al.*, 2009]. Furthermore, radon has been considered as a potential earthquake precursor [Virk and Singh, 1994; Igarashi *et al.*, 1995]. However, most of the reported observations have highlighted contradictory signals [e.g., Ghosh *et al.*, 2009] and remain questionable in many aspects [Geller, 2011]. It is generally accepted that earthquake results from a sudden rupture of the crust due to the gradual increase of tectonic stress [e.g., Scholz, 2002]. Coseismic mechanical and possible thermal processes induce sudden changes of the hydraulic properties of the fault zone [Miller *et al.*, 2004; Manga *et al.*, 2012]. All these changes may allow the degassing of volatile elements or affect the natural release of fluid if already present [e.g., Toutain and Baubron, 1999]. However, these effects on the radon emanation from rocks are still poorly understood under upper crustal conditions.

Laboratory experiments under controlled conditions can provide interesting insights. First, the effect of stress on radon emanation has been studied using uniaxial experiments on radium-rich rocks using punctual [Tuccimei *et al.*, 2010; Mollo *et al.*, 2011] and continuous radon measurements [Holub and Brady, 1981; Scarlato *et al.*, 2013]. These studies have shown that radon emanation decreases during the elastic loading phase and is maximal after failure. Between these two stages, i.e., when the increase of stress induces irreversible damage, the radon emanation either decreases or does not change significantly [Mollo *et al.*, 2011]. However, the association of confined pressure conditions and controlled pore fluid pressure may lead to new information. Second, high temperature can influence radon emanation, as evidenced in hydrothermal and metamorphic regions [Girault *et al.*, 2012]. In the laboratory, the heating of U-bearing minerals, sediments, and clay samples has shown an irreversible decrease of radon emanation above a given temperature threshold [Garver and Baskaran, 2004; Jobbágy *et al.*, 2009; Sas *et al.*, 2012]. However, no experiment has been reported on granite, the major constituent of the upper continental crust. In this paper, we report new laboratory experiments on four different granites. First, radon emanation from thermally and mechanically fractured samples was compared with that from intact samples. Second, a new setup placing the sample under natural conditions was used to investigate radon release during mechanical damage.

### 2. Samples Description

Four granites (porosity 1%) were studied (Table 1): a leucogranite (LG), Ailsa Craig (AC), La Peyratte (LP), and Westerly (W). Average grain size was determined by optical microscopy. LG shows the highest average grain

**Table 1.** Petrophysical Properties, Composition, and Radon Parameters of the Granites

Sample Name	Rock Type, Location (Average Grain Size)	Location of Analyses	<sup>232</sup> Th (ppm)	<sup>238</sup> U (ppm)	<sup>226</sup> Ra (Bq kg <sup>-1</sup> )	<sup>226</sup> Ra/ <sup>238</sup> U	<i>E</i> <sub>Ra</sub> (Bq kg <sup>-1</sup> )	Intact Sample	Radon Emanation Coefficient <i>E</i> (%) (Difference Against Intact)		
									Mechanically Fractured	Thermally Fractured	550°C
LG	Leucogranite, Portugal (2000 ± 400 μm)	Bulk rock	20.3	23.9	310	0.50	33.3 ± 1.7	10.75 ± 0.36	10.61 ± 0.71 (-1.3 ± 0.1%)	7.31 ± 0.47 (-32 ± 2%)	1.140 ± 0.033 (-89 ± 4%)
		Quartz-feldspar		8.2	120						
		K-feldspar		7.4	100						
		Muscovite		13.6	190						
		Biotite with traces of chlorite		52.0	970						
AC	Ailsa Craig granite, Scotland (20 ± 4 μm)	Bulk rock	19.4	4.9	60	0.47	5.42 ± 0.40	9.03 ± 0.66	10.63 ± 0.72 (+18 ± 2%)	5.36 ± 0.50 (-35 ± 4%)	0.245 ± 0.085 (-97 ± 34%)
LP	La Peyratte granite, France (200 ± 40 μm)	Bulk rock	n.m. <sup>a</sup>	3.1	60	0.74	2.78 ± 0.22	4.63 ± 0.37	4.92 ± 0.31 (+6.3 ± 0.6%)	2.78 ± 0.35 (-34 ± 5%)	1.91 ± 0.17 (-59 ± 3%)
		Quartz-feldspar		3.2	50						
		Feldspar		2.2	30						
		Biotite-muscovite		12.6	240						
		60% feldspar, 25% biotite		12.4	200						
W	Westerly granite, USA (500 ± 100 μm)	Bulk rock	29.4	1.3	10	0.30	2.19 ± 0.16	21.9 ± 1.6	22.1 ± 2.9 (+0.9 ± 0.1%)	6.43 ± 0.35 (-72 ± 2%)	2.45 ± 0.60 (-88 ± 22%)
		Quartz-feldspar		0.5	≤10						
		Feldspar		0.1	≤10						
		Biotite		3.0	50						
		Iron oxides and other minerals		14.2	150						

<sup>a</sup>n.m.: Not measured.

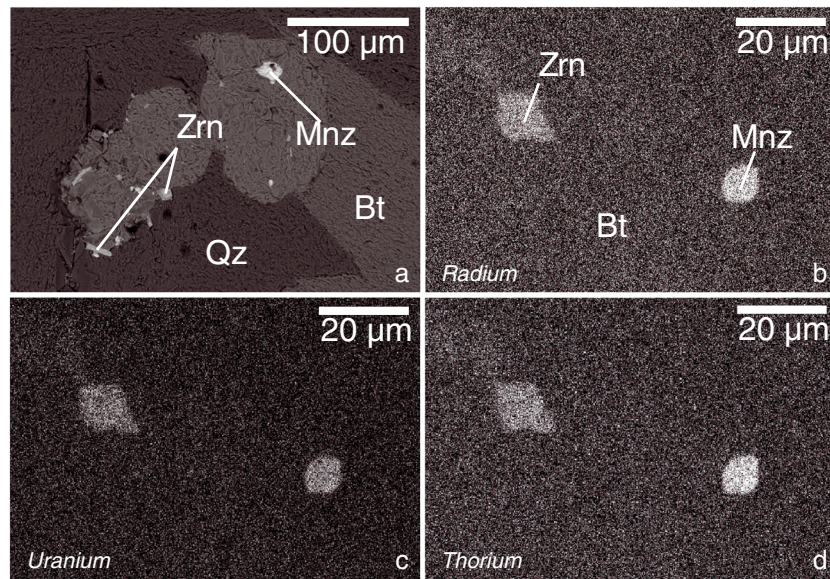


**Figure 1.** (a) Large-scale scanning electron microscope (SEM) image and detailed element mapping analyses of biotites showing high (b) radium, (c) uranium, and (d) thorium concentrations in zircons and monazites for the LG leucogranite. Qz: quartz; Bt: biotite; Mnz: monazite; Zrn: zircon.

size (2000 μm), AC the smallest (20 μm), and LP and W intermediate values of 200 and 500 μm, respectively. Mineralogy was studied with a scanning electron microscope (SEM) and with X-ray diffraction (XRD). <sup>232</sup>Th and <sup>238</sup>U concentrations and <sup>226</sup>Ra concentration were measured on bulk and mineral fractions using high-resolution inductively coupled plasma–mass spectrometry and alpha spectrometry, respectively (Table 1). Energy-dispersive X-ray spectrometry was used to detect radium-rich inclusions in minerals.

While bulk <sup>232</sup>Th concentration remained relatively similar in all samples, bulk <sup>238</sup>U and <sup>226</sup>Ra concentrations varied from 1.3 to 24 ppm and from 10 to 310 Bq kg<sup>-1</sup>, respectively. In general, <sup>238</sup>U, <sup>232</sup>Th, and <sup>226</sup>Ra are mainly concentrated in zircons and monazites entrapped in biotites (Figure 1), which present concentrations in these elements 3–5 times larger than in the bulk sample. The (<sup>226</sup>Ra)/(<sup>238</sup>U) activity ratios of the studied samples, in the range 0.3–0.7, indicate that the uranium decay chain is not at secular equilibrium. Some radium must have been lost relatively to uranium during some open-system processes that could occurred at several time since rock formation. All experiments were performed on cylindrical cores of diameter 4 cm and length 8 cm. Samples were kept at 40°C for at least 1 week before the start of an experiment.

### 3. Experimental Methods

#### 3.1. Radon-222 Emanation From Intact, Thermally, and Mechanically Fractured Samples

Only a fraction of <sup>226</sup>Ra atoms are able to produce <sup>222</sup>Rn atoms that reach the pore space and then the surface of the sample [e.g., Nazaroff, 1992]. This fraction is called the emanation coefficient *E* and depends on the spatial distribution of radium, the properties of the porous network, moisture, and temperature [e.g., Sakoda et al., 2011]. The radon source term (effective radium concentration, *EC<sub>Ra</sub>*), expressed in Bq kg<sup>-1</sup>, is the product of the bulk radium concentration (*C<sub>Ra</sub>*) and *E*. The *EC<sub>Ra</sub>* value of intact, thermally, and mechanically fractured samples were determined in the laboratory using the accumulation method. The sample was placed in an accumulation chamber connected to an intercalibrated ionization chamber (Alphaguard™, Saphymo, Germany), which measured continuously the radon concentration in-growth *C(t)* at 1 h interval following Ferry et al. [2002]. The *EC<sub>Ra</sub>* value was calculated as a function of accumulation time *t* and possible leakage in the experiment using [Perrier and Girault, 2012]

$$EC_{Ra}(t) = \frac{V_a}{m} \frac{C(t)}{1 - e^{-\lambda(1+a_V)t}} (1 + a_V), \quad (1)$$

where *V<sub>a</sub>* is the total air volume available, *m* is the mass of the sample,  $\lambda$  is the decay constant of radon-222 ( $2.1 \times 10^{-6} \text{ s}^{-1}$ ), and  $a_V = \lambda_V/\lambda$  is the normalized leakage rate determined by a least squares fit of the data,

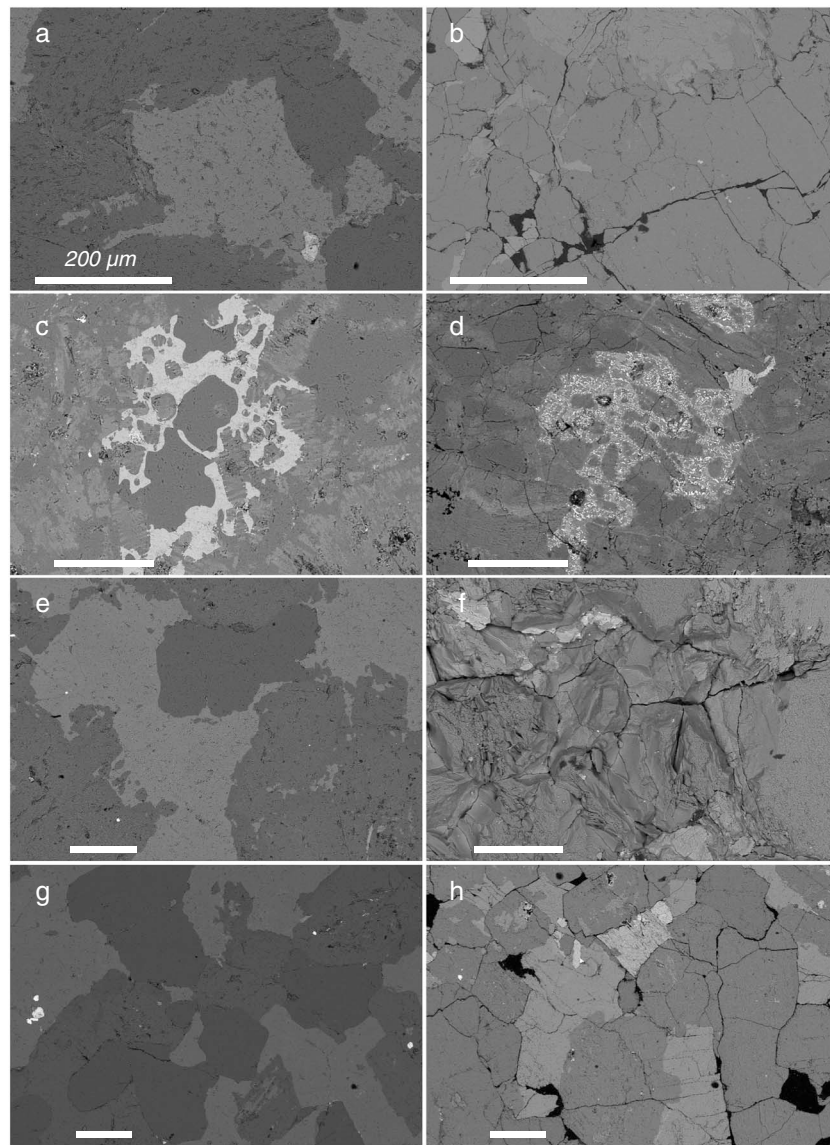


**Figure 2.** SEM images of (a, c, e, and g) intact and (b, d, f, h) 850°C heat-treated granites sorted by decreasing average grain size: from top to bottom, (Figures 2a and 2b) leucogranite (LG), (Figures 2c and 2d) Westerly (W), (Figures 2e and 2f) La Peyratte (LP), and (Figures 2g and 2h) Ailsa Craig (AC).

where  $\lambda_V$  is the volumetric leakage rate. The total uncertainty on  $EC_{Ra}$  (8% on average) corresponds to the punctual uncertainty related to accumulation curve (<1%) and reproducibility (5%), and to the overall absolute uncertainty of the instrument (4%) [Lin *et al.*, 2013]. The emanation coefficient  $E$  was inferred from  $EC_{Ra}/C_{Ra}$ .

Heat treatments were performed with a programmable Meker MHT-3 furnace. Intact samples were heated at a rate of 50°C/h, up to 550°C or 850°C, kept 10 h at the maximal temperature, and then cooled at 50°C/h, to avoid any quenching or thermal shocking effect. All the samples show higher fracture density after heat treatment at 850°C compared with intact samples (Figure 2). This intense microfracturing, increasing the crack surface area and permeability of the sample [Darot *et al.*, 1992], is due to the different thermal expansion coefficients of minerals [Fredrich and Wong, 1986], the  $\alpha$ - $\beta$  transformation of quartz above 550°C [Glover *et al.*, 1995], and the melting of biotites above 750°C [Le Breton and Thompson, 1988]. Determination of  $EC_{Ra}$  was launched the day after the heat treatment.

Mechanical fracturing was performed using the triaxial cell installed at École Normale Supérieure (France) (Figure 3a). Details on this experimental setup are given in Brantut *et al.* [2011] and Ougier-Simonin *et al.*

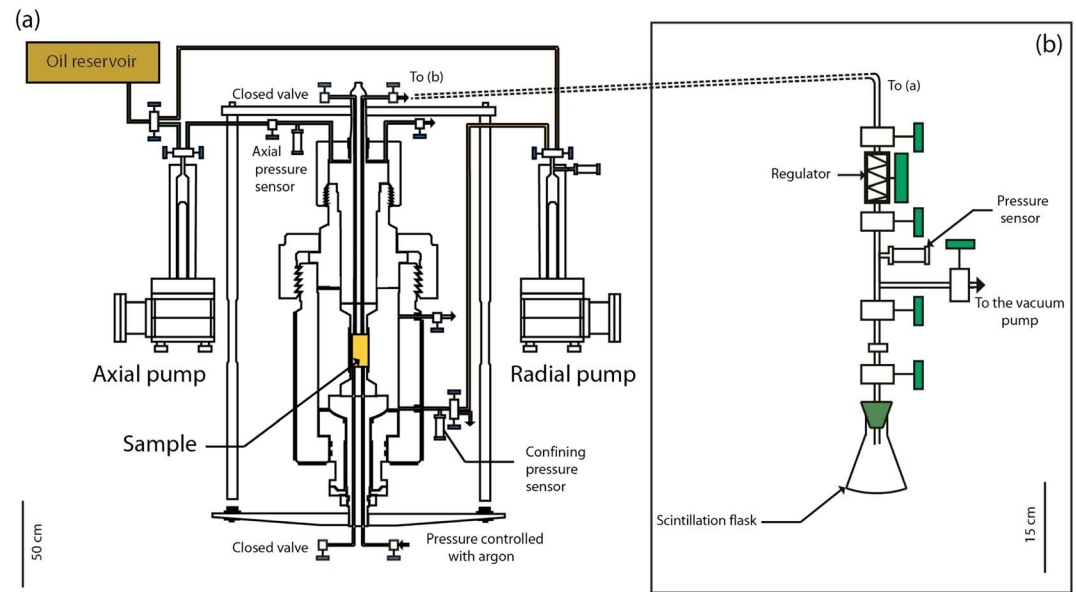


**Figure 3.** Simplified schematics of (a) the triaxial cell (modified from *Passelègue et al.* [2013]) and (b) the gas sampling device.

[2011]. Intact samples were mechanically fractured by linearly increasing differential stress until the macroscopic rupture at a confining pressure of 20 MPa without any pore fluid pressure. Radon emanation measurement started approximately 3 h after the rupture.

### 3.2. Continuous Radon-222 Measurement During Differential Stress Cycles Under Confinement

A 1 month long continuous radon release experiment was conducted on a 550°C heated LG sample under triaxial conditions and under closed system configuration (Figure 3a). During the experiment, passive acoustic emissions were recorded and active  $P$  wave velocity surveys were performed, both using a high-frequency acoustic monitoring system [Brantut et al., 2011]. Axial strain was measured with linear variable displacement transducer corrected to account for the apparatus stiffness.

The constant pore pressure of 1 MPa was controlled by argon flow at the bottom of the sample. Argon gas permeates through the sample, and at the time of the sampling, argon is released at the top of the cell toward the pore gas sampling device (Figure 3b). This device includes a pressure regulator and a pressure sensor. Pore gas sampling was performed each day with a prevacuumed scintillation flask of 125 mL (Algade, France). The radon concentration in the flask was inferred 3.5 h after sampling using a photomultiplier (CALEN™, Algade, France). The total uncertainty on radon concentration (9% on average) corresponds to the punctual uncertainty dominated by the counting statistics and the dilution correction (5–9%) [Girault and Perrier, 2012], and to the overall absolute uncertainty (5%).

In the experiment, the sample was kept under constant isotropic conditions (no differential stress, confining pressure 20 MPa, i.e., 750–800 m depth) during 21 days. Then, cycles of differential stress were performed at a rate of 10 MPa/min: the sample was loaded to a given differential stress and then directly unloaded to initial isotropic conditions. Pore fluid sampling was done at the end of the cycle, immediately after the unloading of the sample to initial isotropic conditions. The differential stress was increased each day by 50 MPa from 130 MPa (first cycle) to the macroscopic failure of the sample (340 MPa).

## 4. Results

The four intact granites give  $EC_{Ra}$  values from  $2.2 \pm 0.2 \text{ Bq kg}^{-1}$  for W to  $33 \pm 2 \text{ Bq kg}^{-1}$  for LG (Table 1). The radon emanation coefficient  $E$  values are low for LP ( $4.6 \pm 0.4\%$ ), large for W ( $22 \pm 2\%$ ), and intermediate for AC and LG ( $9.0 \pm 0.7\%$  and  $10.8 \pm 0.4\%$ , respectively). An example of the results obtained with LG samples is illustrated in the supporting information (Figure S1).

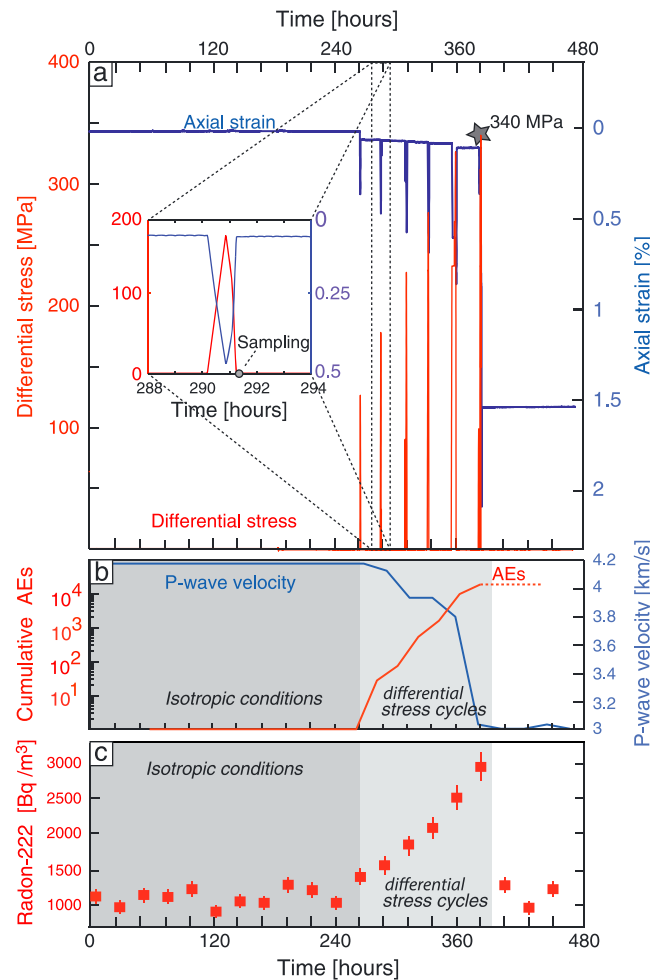


**Figure 4.** Brittle failure of LG granite under 20 MPa confining pressure and 1 MPa pore pressure. (a) Applied differential stress and axial strain, (b) cumulative number of acoustic emissions and *P* wave velocity, and (c) radon-222 concentration are plotted as a function of time. Star corresponds to the macroscopic rupture of the sample. The inset enlarges the second differential stress cycle and shows when the sampling is done.

decreases, the number of acoustic emissions increases and radon concentration significantly increases. Radon concentration rises between  $29 \pm 4\%$  (first cycle) and  $130 \pm 17\%$  (differential stress of 330 MPa). When rupture occurs (340 MPa) the number of acoustic emissions is maximal and the radon concentration is amplified by  $170 \pm 22\%$ . After unloading of the differential stress, radon concentration returns to values similar to those measured before cycles started ( $1150 \pm 150 \text{ Bq m}^{-3}$ ).

### 5. Discussion and Conclusion

The small difference ( $6 \pm 4\%$ ) in radon-222 emanation between intact and macroscopically ruptured granites is consistent with the  $4 \pm 1\%$  difference obtained with tuff samples [Tuccimei et al., 2010]. The small positive difference observed in AC and LP might also be explained by a small value of the radon diffusion coefficient (possibly related to the small average grain size) compared with that of LG and W. This suggests that changes in radon emanation observed after the rupture might not be responsible of potential radon anomalies and that, rather, transient states during the increase of stress need to be studied.

Repeated differential cycles yield a large release of radon, which is maximal near the sample rupture. Differential stress modifies the porous network first by the closing of microcracks, of micropores (e.g., at triple junctions), and then the opening and coalescence of new fractures, as indicated by the decrease of *P* wave

After heat treatment, *E* decreases for all samples (Table 1). Systematically, the decrease is smaller at 550°C (mean of  $-43 \pm 10\%$ ) and larger at 850°C (mean of  $-83 \pm 8\%$ ) compared with intact samples. As we observed no difference between measurements taken immediately after heating, 10 days after, nor 30 days after, this gradual reduction of *E* with temperature was irreversible. In detail, however, the behavior of our heat-treated samples is heterogeneous. While LG, AC, and LP show a similar decrease of *E* at 550°C and LG, AC, and W a similar decrease of *E* at 850°C, the effect of heating on *E* is significantly different for W at 550°C and LP at 850°C (Table 1).

Mechanical fracturing yields contrasting results (Table 1). Indeed, after the macroscopic rupture of the sample, the value of *E* slightly increases on average by  $6 \pm 4\%$  compared with intact samples, but, in detail, *E* decreases after the rupture for LG, increases for LP and AC (up to  $18 \pm 2\%$ ), and shows no significant change for W. No change in *EC*<sub>Ra</sub> was detected 1 year after the macroscopic rupture.

Results of the continuous radon measurements on LG under triaxial conditions are shown in Figure 4. Under a 20 MPa pressure, *P* wave velocity and radon concentration are stable around  $4.2 \text{ km s}^{-1}$  and  $1080 \pm 120 \text{ Bq m}^{-3}$ , respectively. During the cycles of differential stress, *P* wave velocity

velocity and the recording of acoustic emissions. Fractures must subsequently connect to the permeable network isolated micropores (possibly fluid inclusions trapped within grains and/or at grain boundaries), which have stored radon at radioactive equilibrium (i.e., a reservoir with high radon concentration). Radon liberated from occluded pores to interconnected cracks can thus be flushed during the experiment, which illustrates that anomalies result from the transient connection (and subsequent depletion) of occluded reservoirs in which radon had reached equilibrium. Therefore, the closer the state of stress from the rupture point, the larger the transient connection into the sample and the larger the radon release.

Thermal fracturing at 550°C and 850°C show significant irreversible reductions of the value of  $E$  for all samples. It is generally accepted [e.g., Fredrich and Wong, 1986; Glover et al., 1995] that heating increases the amount of crack surfaces, crack connectivity, and permeability, which may all increase  $E$ . After heating at 550°C, the  $\alpha$ - $\beta$  transformation of quartz has occurred, initiating the lengthening of cracks, but the decrease of  $E$  is probably due to the annealing of fission, recoil, and alpha tracks [e.g., Garver and Baskaran, 2004]. After heat treatment at 850°C, the biotites show partial to total vitrification, as illustrated in the supporting information (Figure S2) by the darkening and the disappearance of birefringence of biotites in heat-treated LG sample under cross-polarized light [Brearley, 1987]. In addition, XRD analyses of all 850°C heat-treated samples exhibit smaller normalized diffraction peaks of biotite than their respective intact samples, which highlights the partial disappearance of biotites due to melting [Noda et al., 2011]. In LG, AC, and W samples, the decrease of  $E$  is strong because a large fraction of radium may be concentrated in monazites and zircons included in biotites. By contrast, in LP sample, the melting of biotite has a smaller impact on  $E$ , suggesting that radium may be more homogeneously distributed. Therefore, the isolation of radon sources is the main factor controlling the decrease of  $E$  after heat treatment and dominates the crack surface creation and the increase of permeability. This is particularly true in the case of AC, which, albeit initially impermeable ( $<10^{-22} \text{ m}^2$  [Meredith et al., 2012]), experiences a drastic decrease of  $E$  with thermal treatment.

The main advantages of our triaxial cell experiment compared with uniaxial experiments [Tuccimei et al., 2010; Mollo et al., 2011] were that the samples were placed under natural conditions (controlled confinement and pore pressure) and that they were flushed with pore gas. We demonstrated that the transient release of radon has the potential to shed light on the spatial variation of connectivity in rocks. Our laboratory experiments confirm the role of a dual porosity mechanism in transient gas anomalies induced by mechanical forcing, as suggested by Pili et al. [2004] from field measurements. In addition, our experimental results can bring insights into both the positive [Virk and Singh, 1994; Igarashi et al., 1995] and negative [Wakita et al., 1980; King, 1986; Steinitz et al., 2003] radon anomalies prior earthquakes recorded along natural faults. In our study on granites, the deformation processes are almost purely brittle, leading to the progressive opening of cracks which can shift the transient connection. Assuming a constant fluid flow along a fault zone, deformation processes may promote positive radon signal prior earthquakes, particularly at the highest state of stress. This may allow the opening of tensile cracks and fissures into the damage zone [Sibson, 1983; Mitchell and Faulkner, 2008, 2012]. However, most of the rocks located in the upper part of the brittle crust, where radon measurement campaigns are generally conducted, present higher level of porosity than crustal rocks, leading to ductile or plastic deformation processes under pressure, such as compaction due to pore collapse or granular flow. This may promote the reduction of  $E$  due to a decrease of the transient connection of the porous network [Mollo et al., 2011]. Using the new setup presented here, new deformation experiments should be carried out to focus on the transient release of radon from these materials due to discharge of stress and possibly rise of temperature together.

#### Acknowledgments

The authors warmly thank P. Richon for initiating radon measurements, Y. Pinquier for technical help, S. Guillon for discussions about instruments, C. Chopin for advices on mineralogy, and P. Meredith for providing the block of Aïsa Craig granite. The original version of the paper was greatly improved thanks to the thorough reviews of M. Heap and T. Shimamoto. This is a joint research laboratory effort in the framework of the CEA-ENS "Yves Rocard" LRC (France). All data presented in this paper are available on request.

The Editor thanks Michael Heap and Toshihiko Shimamoto for their assistance in evaluating this paper.

#### References

- Brantut, N., A. Schubnel, and Y. Guéguen (2011), Damage and rupture dynamics at the brittle-ductile transition: The case of gypsum, *J. Geophys. Res.*, *116*, B01404, doi:10.1029/2010JB007675.
- Brearley, A. J. (1987), An experimental and kinetic study of the breakdown of aluminous biotite at 800°C: Reaction microstructures and mineral chemistry, *Bull. Mineral.*, *110*(5), 513–532.
- Cigolini, C., M. Laiolo, and D. Coppola (2007), Earthquake-volcano interactions detected from radon degassing at Stromboli (Italy), *Earth Planet. Sci. Lett.*, *257*, 511–525.
- Darot, M., Y. Guéguen, and M.-L. Baratin (1992), Permeability of thermally cracked granite, *Geophys. Res. Lett.*, *19*, 869–872, doi:10.1029/92GL00579.
- Ferry, C., P. Richon, A. Beneito, J. Cabrera, and J.-C. Sabroux (2002), An experimental method for measuring the radon-222 emanation factor in rocks, *Radiat. Meas.*, *35*, 579–583.
- Fredrich, J. T., and T.-F. Wong (1986), Micromechanics of thermally induced cracking in three crustal rocks, *J. Geophys. Res.*, *91*(B12), 12,743–12,764, doi:10.1029/JB091iB12p12743.

- Garver, E., and M. Baskaran (2004), Effects of heating on the emanation rates of radon-222 from a suite of natural minerals, *Appl. Radiat. Isot.*, *61*, 1477–1485.
- Geller, R. J. (2011), Shake-up time for Japanese seismology, *Nature*, *472*, 407–409.
- Ghosh, D., A. Deb, and R. Sengupta (2009), Anomalous radon emission as precursor of earthquake, *J. Appl. Geophys.*, *69*, 67–81.
- Girault, F., and F. Perrier (2012), Measuring effective radium concentration with large numbers of samples. Part I—Experimental method and uncertainties, *J. Environ. Radioact.*, *113*, 177–188.
- Girault, F., F. Perrier, A. P. Gajurel, M. Bhattarai, B. P. Koirala, L. Bollinger, M. Fort, and C. France-Lanord (2012), Effective radium concentration across the Main Central Thrust in the Nepal Himalayas, *Geochim. Cosmochim. Acta*, *98*, 203–227.
- Glover, P. W. J., P. Baud, M. Darot, P. G. Meredith, S. A. Boon, M. Le Ravalec, S. Zoussi, and T. Reuschlé (1995),  $\alpha/\beta$  phase transition in quartz monitored using acoustic emissions, *Geophys. J. Int.*, *120*, 775–782.
- Holub, R. F., and B. T. Brady (1981), The effect of stress on radon emanation from rock, *J. Geophys. Res.*, *86*(B3), 1776–1784, doi:10.1029/JB086iB03p01776.
- Igarashi, G., S. Saeki, N. Takahata, K. Sumikawa, S. Tasaka, Y. Sasaki, M. Takahashi, and Y. Sano (1995), Ground-water anomaly before the Kobe earthquake in Japan, *Science*, *269*, 60–61.
- Jobbágy, V., J. Somlai, J. Kovács, G. Szeiler, and T. Kovács (2009), Dependence of radon emanation of red mud bauxite processing wastes on heat treatment, *J. Hazard. Mater.*, *172*, 1258–1263.
- King, C.-Y. (1986), Gas geochemistry applied to earthquake prediction: An overview, *J. Geophys. Res.*, *91*(B12), 12,269–12,281, doi:10.1029/JB091iB12p12269.
- Le Breton, N., and A. B. Thompson (1988), Fluid-absent (dehydration) melting of biotite in metapelites in the early stages of crustal anatexis, *Contrib. Mineral. Petrol.*, *99*, 226–237.
- Lin, C.-F., J.-J. Wang, S.-J. Lin, and C.-K. Lin (2013), Performance comparison of electronic radon monitors, *Appl. Radiat. Isot.*, *81*, 238–241.
- Manga, M., I. Beresnev, E. E. Brodsky, J. E. Elkhoury, D. Elsworth, S. E. Ingebritsen, D. C. Mays, and C.-Y. Wang (2012), Changes in permeability caused by transient stresses: Field observations, experiments, and mechanisms, *Rev. Geophys.*, *50*, RG2004, doi:10.1029/2011RG000382.
- Meredith, P. G., I. G. Main, O. C. Clint, and L. Li (2012), On the threshold of flow in a tight natural rock, *Geophys. Res. Lett.*, *39*, L04307, doi:10.1029/2011GL050649.
- Miller, S. A., C. Collettini, L. Chiaraluce, M. Cocco, M. Barchi, and B. J. P. Kaus (2004), Aftershocks driven by a high pressure CO<sub>2</sub> source at depth, *Nature*, *427*, 724–727.
- Mitchell, T. M., and D. R. Faulkner (2008), Experimental measurements of permeability evolution during triaxial compression of initially intact crystalline rocks and implications for fluid flow in fault zones, *J. Geophys. Res.*, *113*, B11412, doi:10.1029/2008JB005588.
- Mitchell, T. M., and D. R. Faulkner (2012), Towards quantifying the matrix permeability of fault damage zones in low porosity rocks, *Earth Planet. Sci. Lett.*, *339–340*, 24–31.
- Mollo, S., P. Tuccimei, M. J. Heap, S. Vinciguerra, M. Soligo, M. Castelluccio, P. Scarlato, and D. B. Dingwell (2011), Increase in radon emission due to rock failure: An experimental study, *Geophys. Res. Lett.*, *38*, L14304, doi:10.1029/2011GL047962.
- Nazaroff, W. W. (1992), Radon transport from soil to air, *Rev. Geophys.*, *30*, 137–160, doi:10.1029/92RG00055.
- Noda, H., K. Kanagawa, T. Hirose, and A. Inoue (2011), Frictional experiments of dolerite at intermediate slip rates with controlled temperature: Rate weakening or temperature weakening?, *J. Geophys. Res.*, *116*, B07306, doi:10.1029/2010JB007945.
- Ougier-Simonin, A., Y. Guéguen, J. Fortin, A. Schubnel, and F. Bouyer (2011), Permeability and elastic properties of cracked glass under pressure, *J. Geophys. Res.*, *116*, B07203, doi:10.1029/2010JB008077.
- Passelègue, F. X., A. Schubnel, S. Nielsen, H. S. Bhat, and R. Madariaga (2013), From sub-Rayleigh to supershear ruptures during stick-slip experiments on crustal rocks, *Science*, *340*(6137), 1208–1211.
- Perrier, F., and F. Girault (2012), Measuring effective radium concentration with less than 5 g of rock or soil, *J. Environ. Radioact.*, *113*, 45–56.
- Perrier, F., et al. (2009), A direct evidence for high carbon dioxide and radon-222 discharge in Central Nepal, *Earth Planet. Sci. Lett.*, *278*, 198–207.
- Pili, E., F. Perrier, and P. Richon (2004), Dual porosity mechanism for transient groundwater and gas anomalies induced by external forcing, *Earth Planet. Sci. Lett.*, *227*, 473–480.
- Richon, P., J.-C. Sabroux, M. Halbwachs, J. Vandemeulebrouck, N. Poussielgue, J. Tabbagh, and R. Punongbayan (2003), Radon anomaly in the soil of Taal volcano, the Philippines: A likely precursor of the M 7.1 Mindoro earthquake (1994), *Geophys. Res. Lett.*, *30*(9), 1481, doi:10.1029/2003GL016902.
- Sakoda, A., Y. Ishimori, and K. Yamaoka (2011), A comprehensive review of radon emanation measurements for mineral, rock, soil, mill tailing and fly ash, *Appl. Radiat. Isot.*, *69*, 1422–1435.
- Sas, Z., J. Somlai, G. Szeiler, and T. Kovács (2012), Radon emanation and exhalation characteristic of heat-treated clay samples, *Radiat. Protect. Dosim.*, *152*(1–3), 51–54.
- Scarlato, P., P. Tuccimei, S. Mollo, M. Soligo, and M. Castelluccio (2013), Contrasting radon background levels in volcanic settings: Clues from <sup>220</sup>Rn activity concentrations measured during long-term deformation experiments, *Bull. Volcanol.*, *75*, 751.
- Scholz, C. H. (2002), *The Mechanics of Earthquakes and Faulting*, 504 pp., Cambridge Univ. Press, Cambridge, U. K.
- Sibson, R. H. (1983), Continental fault structure and the shallow earthquake source, *J. Geol. Soc. London*, *140*, 741–767.
- Steinitz, G., Z. B. Begin, and N. Gazit-Yaari (2003), Statistically significant relation between radon flux and weak earthquakes in the Dead Sea rift valley, *Geology*, *31*(6), 505–508.
- Toutain, J.-P., and J.-C. Baubron (1999), Gas geochemistry and seismotectonics: A review, *Tectonophysics*, *304*, 1–27.
- Trique, M., P. Richon, F. Perrier, J.-P. Avouac, and J.-C. Sabroux (1999), Radon emanation and electric potential variations associated with transient deformation near reservoir lakes, *Nature*, *399*, 137–141.
- Tuccimei, P., S. Mollo, S. Vinciguerra, M. Castelluccio, and M. Soligo (2010), Radon and thoron emission from lithophysae-rich tuff under increasing deformation: An experimental study, *Geophys. Res. Lett.*, *37*, L05305, doi:10.1029/2009GL042134.
- Virk, H. S., and B. Singh (1994), Radon recording of Uttarkashi earthquake, *Geophys. Res. Lett.*, *21*, 737–740, doi:10.1029/94GL00310.
- Wakita, H., Y. Nakamura, K. Notsu, M. Noguchi, and T. Asada (1980), Radon anomaly: A possible precursor of the 1978 Izu-Oshima-kinkai earthquake, *Science*, *207*, 882–883.